A study of fractional Oldroyd-B fluid flow in a ciliated tube

Khadija Maqbool[a], Hajra Ansar[a], Amer Bilal Mann[b,1], Sébastien Poncet[c]

[a]Department of Mathematics & Statistics, International Islamic University, Islamabad 44000, Pakistan.

[b]Department of Mathematical Sciences, Federal Urdu University of Arts, Sciences & Technology, Near Bahria Enclave, Sector C-2, Islamabad 44000, Pakistan.

[c]Mechanical Engineering Department, Université de Sherbrooke, Sherbrooke (QC), J1K2R1 Canada.

[1]Corresponding Author Email: amer.bilal@fuuast.edu.pk **(Amer Bilal Mann)**

Abstract: This study presents a mathematical model for the fractional Oldroyd-B fluid flow through a ciliated tube. The proposed model simulates the movement of mucus (fractional Oldroyd-B fluid) within the respiratory tract, where symplectic and antiplectic metachronal wave patterns are generated by ciliary motion. The model, though intricate, is simplified using the lubrication approach, and the resulting partial differential Equations (pdes) are solved using the fractional Adomian Decomposition Method (ADM). For the analysis of fluid flow, mathematical expressions for the pressure gradient, pressure rise, frictional force, and streamlines are derived, plotted, and discussed. The graphical results demonstrate that the symplectic wave pattern is more effective than the antiplectic wave pattern in transporting mucus through the respiratory tract.

Keywords: Fractional Oldroyd-B fluid; Ciliated tube; Metachronal waves; Fractional differential Equations; ADM;

1. Introduction

Cilia motion is of paramount importance in the physiology of almost all species in the animal and plant kingdoms. Cilia are mainly of two types: motile and non-motile (or primary) cilia, with the internal architectures of motile and non-motile cilia being 9+2 and 9+0, respectively. Cilia serve two main functions in the body: detection and the propulsion of fluids and cells within various organs of humans, animals, or plants [1]. Primary (non-motile) cilia are present in the ears, eyes, kidneys, lungs, and brain, and are responsible for detecting the mechanical and chemical signals communicated by these organs to the brain. In contrast, motile cilia play a significant role in respiration (mucus flow), successful pregnancy, locomotion, alimentation, and circulation in mammals. [2,3,4].

Nowadays, other interesting applications of micro-sized cilia have been found in biochemistry (testing samples of blood, sputum, and urine placed in drops on a chip), acoustic detection, and the sensing and detection of chemicals in the environment using micro-sized sensors [5]. Wang et al. [6] established a cost-effective technique for the fabrication of artificial cilia in the form of micro-sized beads with a polymer coating. Another important application of these microfluidic systems containing cilia is in micromixers [7, 8]. The development of artificial cilia on a chip is a hard nut to crack, and generating oscillations in the cilia when subjected to a magnetic field poses further complications, which have been addressed in the work of Hanasoge et al. [9].

In this study, we investigate the contribution of ciliary motion to the movement of mucus in the trachea. The motile cilia responsible for mucociliary clearance (MCC) have a complex internal structural architecture [1, 10]. More recently Su et al [11] presented a detailed and significant analysis of the role of motile cilia in relation to the recent worldwide coronavirus pandemic. Cilia beat in a coordinated and periodic pattern, and the hydrodynamic interactions among the cilia occur due to phase differences in their beating, generating metachronal waves [12]. It is also noteworthy that all ciliary activity results from hydrodynamic interactions among the cilia, their surrounding cells, and biofluids. The recent detailed work on ciliary hydrodynamics may be credited to Javid et al., [13] and Guo et al., [14]. There are various patterns of ciliary motion, such as effective strokes, recovery strokes, planar motion, flickering, stiff beating, low-amplitude beating, and very large circling motion [15]. Marino and Aiello [16] found the ciliary beat frEquationuency of human bronchial cilia to be 15.6 Hz at 34 0 C which tend to decrease as the

temperature decreases.

Cilia driven mucous flow is a naturally occurring phenomenon which has recently been the focus of interest of experimental verification because of its practical application in human respiratory channel. To name a few only, in vitro cell culture investigations carried out by Matsui et al. [17] reported that mucous flow assumes the shape of large circles in human airways. Khelloufi et al. [18] observed that swirling patterns in mucous flow are the results of circular motion of cilia mats lying under the mucous and the sizes of these swirling patterns vary with the density of cilia. More recently, Gsell et al. [19] noted that due to invasive nature of invivo experiments, mechanism of mucous flow due to ciliary activity is not fully understood and hence further investigations are desirable to completely understand this biophysical process. They [19] further made a significant contribution by experimentally verifying that there is strong hydrodynamic connection between the mucous flowing in the human bronchial epithelium and the movement of cilia involved in this process. They also modeled the motion of cilia in the human bronchial epithelium as a 2 dimensional flow model in which cilia are aligned according to stream-wise alignment rule. Gsell et al. [19] treated mucous as a Newtonian fluid for which the Navier-Stokes Equations are developed and then solved numerically by using Bhatnagar-Gross- Krook lattice-Boltzmann method on a hexagonal unit elements (having diameter 10 to 20 $\grave{\imath}m$ in which there are groups of 5 to 15 cells) for (i) multiciliated cells (ii) club and goblet cells. For details of this practical application of cilia motion we refer the readership to [19]

More recently, Sedaghat et al. [20] studied the MCC by approximating the mucous as a Giesekus fluid which is capable of capturing shear thinning effect and the first and second normal stress differences in shear flows. Sedaghat et al. [21] further examined the complicated cilia driven mucous flow problem by approximating the lung mucous as a 5-mode nonlinear Giesekus model in which periciliary layer has been treated as a Newtonian fluid and the mucous above this layer as a non-Newtonian fluid . The key findings of [21] may be considered important in studies analyzing MCC rate issues.

Mucus is represented by a fractional Oldroyd-B fluid model in this paper and MCC critically depends upon the ciliary motion, serous fluid properties, viscoelasticity and the adhesiveness with the bronchial tract of mammals. Viscoelastic fluid models in MCC has been considered in [15] and is observed that ciliary function is dependant upon mucous gel, periciliary hydration, temperature, mucous loading and operating frEquationuency of cilia. It is a fact that mucous flow

depends upon its viscoelastic behavior but due to mathematical complexity, researchers considered mucous as a Newtonian fluid [22] and as a shear thinning non-Newtonian fluids [23, 24, 25]. Few studies [26, 27] have discussed the viscoelastic behavior of mucous. Oldroyd-B [28] with his coresearchers developed a frame-invariant constitutive Equationuation because it can explain all local and non local behavior of mucous.

Fractional calculus [29] plays a prominent role in modern day medical science and medicines [30]. Fractional model is considered in this study because of the fact that cilia is a microscopic structure and its motion, functioning and various other characteristics in the respiratory and reproductive systems of humans/mammals can be better under-stood by using fractional order derivatives i.e., in the range from zero to unity. Recently much interest has been evolved in studying the fractional non-linear pdes and a variety of methods like Adomian decomposition method (ADM) [31], reduced differential transform nethod (RDTM) [32], modified decomposition method (MDM) [33], artificial neural networks (ANNs) [34] have been applied to obtain a semi-analytic solutions. More recently Altawallbeh et al. [35] introduced and applied generalized Riccati simple Equationuation method (GRSEM) to study nonlinear pde containing time fractional derivatives occuring in generalized nematic liquid crystals system and Az-Zo'bi et al [36] applied the same technique for the solution of conformable generalized Kudryashov Equationuation of pulses propagation.

This study models mucus flow (as an Oldroyd-B fluid) in a ciliated tube, using the envelope model [37, 38] to address challenges in simulating MCC that numerical solvers fail to capture. ADM [33] is applied, effectively simulating mucus flow in the human trachea, driven by ciliary motion under a low Reynolds number, long-wavelength approximation [39].

The novelty of this study lies in the fact that, to the best of the authors' knowledge, no prior research has examined mucus flow in the respiratory tract using a fractional Oldroyd-B model within a ciliated tube, incorporating both symplectic and antiplectic wave patterns. The Oldroyd-B model, a viscoelastic model accounting for both relaxation and retardation time effects, closely aligns with mucus flow, as the viscosity and elasticity of mucus vary over time due to external conditions, composition, and applied mechanical forces. Mathematically, this study is significant because (i) the nonlinear partial differential Equations involved rEquationuire careful analysis and are solvable via the lubrication approach, and (ii) analytical expressions for the stream function, pressure, and velocity are derived, enabling the evaluation of frictional forces on the

ciliated tube's surface, which could be a breakthrough for bioengineering.

2. Mathematical Model

The regime considered is shown in Fig. 1 and comprises a circular tube of length L. The inner tube is circular and collective cilia beating generates the metachronal waves and fluid flow. The geometry of ciliated tube can be simulated by the following equations [27].

$$\overline{R} = \overline{H} = \overline{f}_1\left(\overline{Z},\bar{t}\right) = a\varepsilon\cos\left[\frac{2\pi}{\lambda}\left(\overline{Z} - c\bar{t}\right)\right] + a, \qquad (1)$$

$$\overline{Z} = \overline{f}_2\left(\overline{Z},\overline{Z}_{0,}\bar{t}\right) = a\varepsilon\sin\left[\frac{2\pi}{\lambda}\left(\overline{Z} - c\bar{t}\right)\right] + a, \qquad (2)$$

No slip condition implies that fluid velocities due to cilia tips satisfy the following conditions:

$$\overline{U} = \overline{R}_{\bar{t}}\Big|_{Z=Z_0} = \overline{f}_{1\bar{t}} + \overline{f}_{1\overline{Z}}\,\overline{Z}_{\bar{t}} = \overline{f}_{1\bar{t}} + \overline{f}_{1\overline{Z}}\,\overline{W} \qquad (3)$$

and

$$\overline{W} = \overline{Z}_{\bar{t}}\Big|_{Z=Z_0} = \overline{f}_{2\bar{t}} + \overline{f}_{2\overline{Z}}\,\overline{Z}_{\bar{t}} = \overline{f}_{2\bar{t}} + \overline{f}_{2\overline{Z}}\,\overline{W}, \qquad (4)$$

where the alphabetical subscripts denote the partial derivatives with respect to the respective subscripts. Using Equations $(1-2)$ in Equations $(3-4)$, one obtains the following expressions:

$$\overline{U} = \frac{\frac{2\pi}{\lambda}\left(ac\varepsilon\sin\left[\frac{2\pi}{\lambda}\right]\left(\overline{Z} - c\bar{t}\right)\right)}{1 - \frac{2\pi}{\lambda}\left(ea\varepsilon\cos\left[\frac{2\pi}{\lambda}\right]\left(\overline{Z} - c\bar{t}\right)\right)} \qquad (5)$$

and

$$\overline{W} = \frac{\frac{-2\pi}{\lambda}\left(eac\varepsilon\cos\left[\frac{2\pi}{\lambda}\right]\left(\overline{Z} - c\bar{t}\right)\right)}{1 - \frac{2\pi}{\lambda}\left(ea\varepsilon\cos\left[\frac{2\pi}{\lambda}\right]\left(\overline{Z} - c\bar{t}\right)\right)}. \qquad (6)$$

The constitutive Equation for fractional Oldroyd-B fluid is governed by:

$$\left(1+\lambda_1^{\alpha}\frac{\partial^{\alpha}}{\partial t^{\alpha}}\right)\overline{S}=\mu\left(1+\theta_1^{\beta}\frac{\partial^{\beta}}{\partial t^{\beta}}\right)A_1, \qquad (7)$$

Where α and β are the fractional parameters with $0<\alpha\le\beta\le 1$. When $\alpha=\beta=1$ then this model represents Oldroyd-B model which can be see in [40]. When $\lambda_1=0$ and $\alpha=\beta=1$, the present model reduces to Maxwell fluid model and if $\lambda_1=\theta_1=0$, then it depicts the classical Navier-Stokes model thus validates the applicability of this model. Thus governing Equationuation of motion becomes:

$$\overline{U}_{\overline{R}}+\overline{W}_{\overline{Z}}+\frac{\overline{U}}{\overline{R}}=0, \qquad (8)$$

$$\rho\overline{U}_{\overline{t}}+\overline{U}\,\overline{U}_{\overline{R}}+\overline{W}\,\overline{U}_{\overline{Z}}=-\overline{P}_{\overline{R}}+\frac{1}{\overline{R}}\left(\overline{R}\,\overline{S}_{\overline{R}\overline{R}}\right)_{\overline{R}}+\left(\overline{S}_{\overline{R}\overline{Z}}\right)_{\overline{Z}} \qquad (9)$$

and

$$\rho\overline{W}_{\overline{t}}+\overline{U}\,\overline{W}_{\overline{R}}+\overline{W}\,\overline{W}_{\overline{Z}}=-\overline{P}_{\overline{Z}}+\frac{1}{\overline{R}}\left(\overline{R}\,\overline{S}_{\overline{R}\overline{Z}}\right)_{\overline{R}}+\left(\overline{S}_{\overline{Z}\overline{Z}}\right)_{\overline{Z}}. \qquad (10)$$

The moving and fixed frames are connected via the transformations

$$\overline{r}=\overline{R},\ \overline{z}=\overline{Z}-c\overline{t},\ \overline{u}=\overline{U},\ \overline{w}=\overline{W}-c. \qquad (11)$$

By introducing the dimensionless variables as:

$$\begin{aligned} &r=\frac{\overline{r}}{a},\ z=\frac{\overline{z}}{\lambda},\ w=\frac{\overline{w}}{c},\ p=\frac{a^2\overline{p}}{c\lambda\mu},\ u=\frac{\lambda\overline{u}}{ac},\\ &t=\frac{c\overline{t}}{\lambda},\ \beta=\frac{a}{\lambda},\ \mathrm{Re}=\frac{\rho ca}{\mu},\ \lambda_1=c\frac{\overline{\lambda_1^{\alpha}}}{\lambda},\ \theta_1^{\beta}=c\frac{\overline{\theta_1^{\beta}}}{\theta_1}, \end{aligned} \qquad (12)$$

where Re is the Reynolds number. Introducing Equations (11-12) and the approximations $\left(\mathrm{Re}\to 0,\ \lambda\to\infty\right)$ [38], Equation (9) reduces to:

$$\frac{\partial p}{\partial r}=0, \qquad (13)$$

implies that $p\neq p(r)$ and Equation (10) reduces to:

$$\frac{\partial p}{\partial z}=\frac{dp}{dz}=\frac{1}{r}\frac{\partial}{\partial r}\left(rS_{rz}\right) \qquad (14)$$

Multiplying $\left(1+\lambda_1^{\alpha}\frac{\partial^{\alpha}}{\partial t^{\alpha}}\right)$ on both sides of Equation (14) will yield to:

$$\left(1+\lambda_1^{\alpha}\frac{\partial^{\alpha}}{\partial t^{\alpha}}\right)\frac{dp}{dz}=\frac{1}{r}\frac{\partial}{\partial r}\left(r\left(1+\lambda_1^{\alpha}\frac{\partial^{\alpha}}{\partial t^{\alpha}}\right)S_{rz}\right), \qquad (15)$$

where

$$\left(1+\lambda_1^{\alpha}\frac{\partial^{\alpha}}{\partial t^{\alpha}}\right)S_{rz}=\left(1+\theta_1^{\beta}\frac{\partial^{\beta}}{\partial t^{\beta}}\right)\frac{\partial w}{\partial r}. \qquad (16)$$

Using Equation (16) in Equation (15) will result in:

$$\left(1+\lambda_1^{\alpha}\frac{\partial^{\alpha}}{\partial t^{\alpha}}\right)\frac{dp}{dz}=\frac{1}{r}\frac{\partial}{\partial r}\left(r\left(1+\theta_1^{\beta}\frac{\partial^{\beta}}{\partial t^{\beta}}\right)\frac{\partial w}{\partial r}\right). \qquad (17)$$

Twice integration of Equation (17), one gets:

$$C_2 = C_1 \ln r + \frac{r^2}{4}\left(1 + \lambda_1 \frac{\partial^{\alpha}}{\partial t^{\alpha}}\right)\frac{dp}{dz} + \left(1 + \theta_1 \frac{\partial^{\beta}}{\partial t^{\beta}}\right) w(r,z) \qquad (18)$$

where C_1 and C_2 are constants of integration. To find the values of constants C_1 and C_2, following boundary conditions are used.

$$w = \frac{-2\pi\varepsilon\beta_1\cos 2\pi z}{1-2\pi\varepsilon\beta_1\cos 2\pi z} - 1 = w(h) \qquad at\ r = h,$$
$$w_r = 0 \qquad at\ r = 0 \quad \text{where } h = 1+\varepsilon\cos(2\pi z). \qquad (19)$$

After using the values of constants C_1 and C_2, Equation (18) takes the form:

$$\left(1+\theta_1^{\beta}\frac{\partial^{\beta}}{\partial t^{\beta}}\right)\left(w(r,z)-w(h)\right)=\left(1+\lambda_1^{\alpha}\frac{\partial^{\alpha}}{\partial t^{\alpha}}\right)\frac{dp}{dz}\left(\frac{r^2}{4}-\frac{h^2}{4}\right). \qquad (20)$$

Defining the volume flow rate as

$$Q = 2\int_0^h rw\,dr, \qquad (21)$$

and Equation (20) becomes:

$$\frac{-8}{h^4}\left(1+\theta_1^{\beta}\frac{\partial^{\beta}}{\partial t^{\beta}}\right)\left(Q-h^2 w(h)\right)=\left(1+\lambda_1^{\alpha}\frac{\partial^{\alpha}}{\partial t^{\alpha}}\right)\frac{dp}{dz}. \qquad (22)$$

The flux q and the volume flow rate Q are related as:

$$Q = q + h^2, \tag{23}$$

whereas $\overline{Q}$ (dimensionless mean volume flow rate) is computed as:

$$\overline{Q} = \frac{1}{T}\int_0^t Q dt = q + 1 + \frac{\varepsilon^2}{2}, \tag{24}$$

where $T = \frac{\lambda}{c}$ is the complete time period. Using Relations (23 & 24), Equation (22) takes the form:

$$\left(1 + \lambda_1^{\alpha}\frac{\partial^{\alpha}}{\partial t^{\alpha}}\right)\frac{\partial p}{\partial z} = \frac{-8}{h^4}\left(1 + \theta_1^{\beta}\frac{\partial^{\beta}}{\partial t^{\beta}}\right)\left(\overline{Q} - 1 - 0.5\varepsilon^2 - h^2 w(h)\right), \tag{25}$$

or

$$\left(1 + \lambda_1^{\alpha}\frac{\partial^{\alpha}}{\partial t^{\alpha}}\right) f = \left(1 + \theta_1^{\beta}\frac{\partial^{\beta}}{\partial t^{\beta}}\right) A, \tag{26}$$

where

$$A = \frac{-8}{h^4}\left(\overline{Q} - 1 - \frac{1}{2}\varepsilon^2 - h^2 w(h)\right), \tag{27}$$

and

$$f = \frac{dp}{dz}, \tag{28}$$

with starting conditions as:

$$f(x,0) = 0 \text{ and } f_t(x,0) = 0, \tag{29}$$

$$\left(\frac{1}{\lambda_1^{\alpha}} + \frac{\partial^{\alpha}}{\partial t^{\alpha}}\right) f = \left(1 + \theta_1^{\beta}\frac{\partial^{\beta}}{\partial t^{\beta}}\right)\frac{A}{\lambda_1^{\alpha}}. \tag{30}$$

The solution $f(x,t)$ can be expanded as by using the ADM [31] as

$$f(x,t) = \sum_{n=0}^{\infty} f_n(x,t). \tag{31}$$

The zeroth-order solution of Equation (30) is:

$$f_0 = 0. \qquad (32)$$

Integrating Equation (30), one gets:

$$f = J^{\alpha}\left(\frac{-1}{\lambda_1^{\alpha}} f + \left(1+\theta_1^{\beta}\frac{\partial^{\beta}}{\partial t^{\beta}}\right)A^{'}\right), \qquad (33)$$

$$A^{'} = \frac{A}{\lambda_1^{\alpha}}, \qquad (34)$$

Using Equation (31) in Equation (33), one obtains the following recursive relation:

$$f_n = J^{\alpha}\left(\frac{-1}{\lambda_1^{\alpha}} f_{n-1} + \left(1+\theta_1^{\beta}\frac{\partial^{\beta}}{\partial t^{\beta}}\right)A^{'}\right), \qquad n \geq 1, \qquad (35)$$

with

$$J^{\alpha} = \frac{1}{\Gamma(\alpha)}\int_0^t \frac{f(\tau)}{(t-\tau)^{1-\alpha}}\, d\tau, \qquad (36)$$

$$f_1 = A^{'}\left(\frac{t^{\alpha}}{\Gamma(\alpha+1)} + \theta_1^{\beta}\frac{t^{\alpha-\beta}}{\Gamma(\alpha-\beta+1)}\right), \qquad (37)$$

$$f_2 = \frac{-A^{'}}{\lambda_1^{\alpha}}\left(\frac{t^{2\alpha}}{\Gamma(2\alpha+1)} + \theta_1^{\beta}\frac{t^{2\alpha-\beta}}{\Gamma(2\alpha-\beta+1)}\right) + A^{'}\left(\frac{t^{\alpha}}{\Gamma(\alpha+1)} + \theta_1^{\beta}\frac{t^{\alpha-\beta}}{\Gamma(\alpha-\beta+1)}\right), \qquad (38)$$

and

$$f_n = A^{'}\left[\sum_{k-1}^{\infty}\left(\frac{(-1)^{k-1}}{\lambda_1^{(k-1)\alpha}}\left(\frac{1}{\Gamma(1+k\alpha)} + \theta_1^{\beta}\frac{t^{-\beta}}{\Gamma(1-\beta+k\alpha)}\right)t^{k\alpha}\right)\right]. \qquad (39)$$

Thus

$$\frac{dp}{dz} = A^{'}\left[\sum_{k-1}^{\infty}\left(\frac{(-1)^{k-1}}{\lambda_1^{(k-1)\alpha}}\left(\frac{1}{\Gamma(1+k\alpha)} + \theta_1^{\beta}\frac{t^{-\beta}}{\Gamma(1-\beta+k\alpha)}\right)t^{k\alpha}\right)\right]. \qquad (40)$$

Multiplying Equation (22) with the factor $\frac{1}{4}(r^2 - h^2)$ will yield to:

$$\frac{1}{4}\left(r^2-h^2\right)\left(1+\lambda_1\frac{\partial^\alpha}{\partial t^\alpha}\right)\frac{\partial p}{\partial z}=\frac{-2}{h^4}\left(r^2-h^2\right)\left(1+\theta_1^\beta\frac{\partial^\beta}{\partial t^\beta}\right)\left(\overline{Q}-h^2w(h)\right). \qquad (41)$$

With the help of Equation (22) and (40), one gets the following expression:

$$w(r,z)=\frac{-2}{h^4}\left(Q-h^2w(h)\right)\left(r^2-h^2\right)+w(h). \qquad (42)$$

As:

$$rw=\frac{\partial\Psi}{\partial r}, \qquad (43)$$

$$-ru=\frac{\partial\Psi}{\partial z}. \qquad (44)$$

Therefore integrating Equation (42), one gets:

$$\int rwdr+g(z)=\Psi, \qquad (45)$$

and

$$\frac{\partial}{\partial z}\int rwdr+g'(z)=\frac{\partial\Psi}{\partial z}. \qquad (46)$$

From Equation (44)

$$\frac{\partial}{\partial z}\int rwdr+g'(z)=-ru, \qquad (47)$$

Or

$$\int rwdr=\frac{-Qr^4}{2h^4}+\frac{Qr^2}{h^2}+\frac{r^4w(h)}{2h^2}-\frac{r^2}{2}w(h), \qquad (48)$$

so that

$$\frac{\partial}{\partial z}\int rwdr=\frac{\partial}{\partial h}\left(\frac{-Qr^4}{2h^4}+\frac{Qr^2}{h^2}+\frac{r^4w(h)}{2h^2}-\frac{r^2}{2}w(h)\right)\frac{\partial h}{\partial z} \qquad (49)$$

and

$$\frac{\partial}{\partial z}\int rwdr=\left(\frac{-2Qr^2}{h^3}+\frac{2Qr^4}{h^5}+\frac{r^4w'(h)}{2h^2}-\frac{r^4w(h)}{h^3}-\frac{r^2}{2}w'(h)\right)\frac{\partial h}{\partial z}. \qquad (50)$$

From Equations (43) and (44), one has:

$$u = \frac{1}{r}\int -r\frac{\partial w}{\partial z}dr, \tag{51}$$

$$\frac{\partial w}{\partial z} = \frac{\partial}{\partial h}\left(\frac{-2}{h^4}\left(Q - h^2 w(h)\right)\left(r^2 - h^2\right) + w(h)\right)\frac{\partial h}{\partial z}, \tag{52}$$

and

$$\frac{\partial w}{\partial z} = \left(\frac{8Qr^2}{h^5} - \frac{4Q}{h^3} + \frac{2r^2 w'(h)}{h^2} - \frac{4r^2 w(h)}{h^3} - w'(h)\right)\frac{\partial h}{\partial z}. \tag{53}$$

Then Equation (51) becomes:

$$u = \left(\frac{-2Qr^3}{h^4} + \frac{2Qr}{h^3} - \frac{r^3 w'(h)}{2h^2} + \frac{r^3 w'(h)}{h^3} + \frac{r}{2}w'(h)\right)\frac{\partial h}{\partial z}, \tag{54}$$

or

$$-ru = \frac{2Qr^4}{h^5} - \frac{2Qr^2}{h^3} + \frac{r^4 w'(h)}{2h^2} - \frac{r^4 w'(h)}{h^3} - \frac{r^2}{2}w'(h). \tag{55}$$

From Equations (47), (50) and (55), one arrives at:

$$g'(z) = 0, \tag{56}$$

so that

$$g(z) = C. \tag{57}$$

Thus Equation (45) becomes:

$$\Psi = \frac{Qr^2}{h^2} - \frac{Qr^4}{2h^4} + \frac{r^4 w(h)}{2h^2} - \frac{r^2}{2}w(h) + C, \tag{58}$$

so that the stream function Ψ is determined and thus by virtue of Equations (43) and (44), complete velocity profile is determined for the problem under consideration. The pressure difference Δp and friction force Fr per wavelength are computed as

$$\Delta p = \int_0^1 \frac{dp}{dz}dz \tag{59}$$

and

$$Fr = -\int_0^1 \left(h(z)\frac{dp}{dz}\right)dz. \tag{60}$$

3. Results and discussion

Table 1 shows that ciliary flow requires the high change in pressure for fractional Oldroyd-B fluid and least for Maxwell fluid. Fractional Oldroyd-B fluid and fractional Maxwell fluid models require more change in pressure as compared to the classical Oldroyd-B and Maxwell fluid models.

The dynamics of the fractional Oldroyd-B fluid flow through a ciliated tube are mainly dependant upon the $\alpha, \beta, \varepsilon, \lambda_1, \theta_1$ and time t. The mathematical results of the pressure gradient, velocity and stream lines are drawn to observe the impacts of involving parameters by fixing $a = 0.4, b = 0.5, Q = 1.5, \varepsilon = 0.1, \lambda_1 = 0.6, \theta_1 = 0.7, \alpha = 0.4$ and $\beta = 0.6$.

Figs. 2a-2b displays the effects of fractional parameters $(\alpha$ and $\beta)$ on Oldroyd-B fluid flow through the ciliated tube. Fig. 2a indicates that when the order of fractional derivative increases then the flow of Oldroyd-B fluid through the ciliated tube requires less change in pressure but Fig. 2b shows that increasing values of fractional order derivative of first Rivlin-Erickson tensor gives increasing effect on pressure gradient. Physically Fractional-order derivatives introduces the memory effects into the fluid and when a pressure gradient is applied, the fractional derivative leads to a slower response in terms of flow development compared to integer-order derivatives, causing a lag in flow. Fractional derivatives often highlight the elastic nature of the fluid more strongly than traditional models and also these can reduce the overall flow resistance, depending on the fractional order. Fig. 2c portrays the increasing effect of ε on pressure gradient i. e., when the cilia length rises more change in pressure is required for the flow of fractional Oldroyd-B fluid. In the physical context of the Oldroyd-B fluid (a viscoelastic fluid) in a tube with cilia, the cilia length can significantly influence the flow and pressure gradient since longer cilia tend to have a greater capacity to propel the fluid, contribute greater shear stresses due to the enhanced fluid-cilia interaction and may cause greater fluid mixing due to their more extensive motion, leading to a more homogeneous flow distribution. The effect of relaxation time λ_1 on pressure gradient is depicted in Fig. 2d, it is noticed that the growing values of λ_1 causes to reduce the change in pressure due to rise in restoring force. Physically the larger values of parameter λ_1 indicates that the fluid retains its elastic memory for a longer period and thus

takes longer to return to its original state after being deformed by forces. The delayed response on stress is measured by the retardation time θ_1 in Fig. 2e, the delayed response shows that pressure gradient decays when the delayed response on stress rises which can be physically interpreted that for larger values of parameter θ_1 that the viscous effects take longer to develop, leading to delayed viscous stress accumulation. This means that even if the pressure gradient is applied, the fluid does not immediately experience a full viscous response and for high retardation times, the flow may become more stable and less sensitive to abrupt changes in the pressure gradient, resulting in a more uniform flow profile. The impact of time on unsteady flow is shown in Fig. 2f which depicts that with the passage of time, flow of fractional Oldroyd-B fluid requires the less amount of pressure gradient.

The flow behaviour is observed through the radial and axial velocity of a fractional Oldroyd-B fluid. Fig. 3a indicates the growing effects of cilia length parameter ε on u, it displays that the length of cilia help to increase the flow in radial direction due to strong deriving force produced by the tips of cilia. Fig. 3b illustrates the variation of Q on radial velocity u. It is noted that the rise in volume flow rate causes to reduce the flow of fractional Oldroyd-B fluid in radial direction. Since volume flow rate is across the radius, therefore reduces the flow in radial direction.

The axial flow for the variation of ε is shown in Fig. 4a. The growing values of cilia length parameter indicates that the axial flow increases with the deriving force due to high length of cilia.

Also axial flow at $r = 0$ is forward but at the tip of cilia it is in reversed direction. Fig. 4b shows that rise in volume flow helps to accelerate the flow in axial direction, it is also observed that volume flow rate works as a booster for the fractional Oldroyd-B fluid in axial direction.

The stream line patterns help to note the flow characteristics of fractional Oldroyd-B fluid. Therefore Figs. 5(a-c) are plotted for stream lines. Figs 5 a-c display that bolus size decreases with the growing values of Q. The size of bolus in (fractional Oldroyd-B fluid) reduces due to its high viscosity in the existence of volume flow rate.

Figs. 6(a-c) display the stream line plots for different values of cilia length parameter ε. These graphs show that size of bolus in fractional Oldroyd-B fluid increases as the cilia length parameter rises and it is due to the large deriving force employed on fluid by the tip of cilia.

Figs. 7(a - b) display the axial flow for different values of ε and Q in symplectic and antiplectic wave configurations. The plots show that symplectic wave pattern gives the high velocity profile in comparison with antiplectic wave pattern. For fast flow of fractional Oldroyd-B fluid, the symplectic wave pattern is suitable choice therefore in this study authors have considered the symplectic wave pattern for the mucous flow.

4. Conclusions

This research describes the dynamics of mucous flow through the tracheobronchial tree. Mucous is considered as a fractional Oldroyd-B fluid and tracheobronchial tube is chosen to be the ciliated tube. Due to the fractional differential model, the investigations under consideration become complex and complexity in mathematical analysis can be overcome by the ADM. Mathematical expressions for pressure gradient, stream function and velocity are evaluated and their effects are displayed through graphs and the following features are observed.

- The pressure gradient decreases with the rising values of fractional parameter α but increases with the growing values of fractional parameter β.
- The relaxation parameter λ_1 help to rise in pressure gradient whereas the retardation time θ_1 causes to reduce the pressure gradient.
- The cilia length ε acts as a deriving force for flow of fractional Oldroyd-B fluid. Therefore the pressure gradient and bolus size rise by increasing cilia length ε.
- The volume flow rate causes to accelerate the axial velocity and decay the radial velocity and the bolus size.
- In this study, authors have ignored the thermal and concentration effects, which will be considered in an upcoming work.

Data Availability Statement

No Data is associated in the manuscript.

References:

[1] Guirao, B., Joanny, J., F., "Spontaneous creation of macroscopic flow and metachronal waves in an array of cilia", Biophys. J., 92 (6), 1900-1917 (2007) DOI: 10.1529/biophysj.106.084897.

[2] Lyons, R. A., Saridogan, E., & Djahanbakhch, O, "The reproductive significance of human Fallopian tube cilia", Human reproduction update, 12 (4), 363-372 (2006) DOI:

https://doi.org/10.1093/humupd/dml012.

[3] Agrawal, H. L., & ANAWARUDDIN, A., "Cilia transport of bio-fluid with variable viscosity", INDIAN JOURNAL OF PURE & APPLIED MATHEMATICS, 15 (10), 1128-1139 (1984).

[4] Shakib Arslan, M., Abbas, Z., & Rafiq, M., Y., "Biological flow of thermally intense cilia generated motion of non-Newtonian fluid in a curved channel", Advances in Mechanical Engineering, 15 (3), 16878132231157179, (2023) DOI: https://doi.org/10.1177/16878132231157179.

[5] Sahadevan, V., Panigrahi, B., & Chen, C. Y. “Microfluidic applications of artificial cilia: recent progress, demonstration, and future perspectives”, Micromachines, 13(5), 735, (2022) DOI: https://doi.org/10.3390/mi13050735.

[6] Wang, Y., Gao, Y., Wyss, H., Anderson, P, D, & den Toonder, J, M, "Out of the cleanroom, self-assembled magnetic artificial cilia", Lab on a Chip, 13 (17), 3360-3366 (2013) DOI: 10.1039/C3LC50458A.

[7] Khatavkar, V. V., Anderson, P. D., den Toonder, J, M, & Meijer, H, E, "Active micromixer based on artificial cilia", Physics of Fluids, 19 (8), (2007) DOI: https://doi.org/10.1063/1.2762206.

[8] den Toonder, J., Bos, F., Broer, D., Filippini, L., Gillies, M., Goede, J, de., Mol, T., Reijme, M., Talen, W., Wilderbeek, H., Khatavkar, V., "Artificial cilia for active micro-fluidic mixing", Lab on a Chip, 8 (4), 533-541 (2008) DOI: https://doi.org/10.1039/B717681C.

[9] Hanasoge, S., Ballard, M., Hesketh, P. J., Alexeev, A., "Asymmetric motion of magnetically actuated artificial cilia", Lab on a Chip, 17(18), 3138-3145 (2017) DOI https://doi.org/10.1039/C7LC00556C.

[10] Krivovichev, G. V., & Tregoubov, V. P.,"Computer modelling of ciliary motility", Acta of Bioengineering and Biomechanics, 10 (3), 61-64, (2008).

[11] Su, Peng., Zhou, Fangfang, Zhang, Long., "Motile cilia and microvillar: accomplices of SARS-CoV-2 in penetrating mucus barrier and infecting airway epithelium", Signal Transduction and Targeted Therapy, 8 (1), 117, (2023) DOI https://doi.org/10.1038/s41392-023-01387-7.

[12] Teff, Z., Priel, Z., & Gheber, L. A., "Forces applied by cilia measured on explants from mucociliary tissue", Biophysical journal, 92 (5), 1813-1823, (2007) DOI:

10.1529/biophysj.106.094698.

[13] Javid, K., Riaz, M., Chu, Yu-Ming, Khan, M, Ijaz, Khan, Samiullah, Kadry, S., "Peristaltic activity for electro-kinetic complex driven cilia transportation through a non-uniform channel", Computer Methods and Programs in Biomedicine, 200, 105926, (2021) DOI: https://doi.org/10.1016/j.cmpb.2020.105926.

[14] Guo, H., Nawroth, J., Ding, Y., Kanso, E., "Cilia beating patterns are not hydrodynamically optimal", Physics of Fluids, 26 (9), (2014) DOI: https://doi.org/10.1063/1.4894855.

[15] Smith, D. J., Gaffney, E. A., Blake, J. R., "Modelling mucociliary clearance", Respiratory physiology & neurobiology, 163 (1-3), 178-188, (2008) DOI: https://doi.org/10.1016/j.resp.2008.03.006.

[16] Marino, M. R., Aiello, E., "Cinemicrographic analysis of beat dynamics of human respiratory cilia", Cell Motility, 2(S1), 35-39, (1982) DOI: https://doi.org/10.1002/cm.970020709.

[17] Matsui, H., Randell, S. H., Peretti, S. W., Davis, C., W., Boucher, R., C., "Coordinated clearance of periciliary liquid and mucus from airway surfaces", The Journal of clinical investigation, 102(6), 1125-1131, (1998) DOI: https://doi.org/10.1172/JCI2687.

[18] Khelloufi, M. K., Loiseau, E., Jaeger, M., Molinari, N., Chanez, P., Gras, D., Viallat, A., "Spatiotemporal organization of cilia drives multiscale mucus swirls in model human bronchial epithelium", Scientific reports, 8 (1), 2447, (2018) DOI: https://doi.org/10.1038/s41598-018-20882-4.

[19] Gsell, S., Loiseau, E., D'Ortona, U, Viallat, A., Favier, J., "Hydrodynamic model of directional ciliary-beat organization in human airways", Scientific reports, 10 (1), 8405, (2020) DOI: https://doi.org/10.1038/s41598-020-64695-w.

[20] Sedaghat, M. H., George, U. Z., Abouali, O., "A nonlinear viscoelastic model of mucociliary clearance", Rheologica Acta, 60 (6), 371-384, (2021) DOI: https://doi.org/10.1007/s00397-021-01274-4.

[21] Sedaghat, M. H., Farnoud, A., Schmid, O., Abouali, O., "Nonlinear simulation of mucociliary clearance: a three-dimensional study", Journal of Non-Newtonian Fluid Mechanics, 300, 104727, (2022) DOI: https://doi.org/10.1016/j.jnnfm.2021.104727.

[22] Modaresi, M. A., & Shirani, E., "Mucociliary clearance affected by mucus--periciliary interface stimulations using analytical solution during cough and sneeze", The European

Physical Journal Plus, 138 (3), 1-18, (2023) DOI: https://doi.org/10.1140/epjp/s13360-023-03796-7.

[23] Shaheen, S., Huang, H., Arain, M. B., Duraihem, Faisal, Z., "Significance of peripheral layer: the case of mucus flow through a ciliated tube using Rabinowitsch model", Computer Methods in Biomechanics and Biomedical Engineering, 1-12, (2023) DOI: 10.1080/10255842.2023.2281892.

[24] Modaresi, M. A., & Shirani, E., "Effects of continuous and discrete boundary conditions on the movement of upper-convected maxwell and Newtonian mucus layers in coughing and sneezing", The European Physical Journal Plus, 137 (7), 846, (2022) DOI: https://doi.org/10.1140/epjp/s13360-023-04256-y.

[25] Vélez-Cordero, J. R., Lauga, E., "Waving transport and propulsion in a generalized Newtonian fluid", Journal of Non-Newtonian Fluid Mechanics, 199, 37-50, (2013) DOI: https://doi.org/10.1016/j.jnnfm.2013.05.006.

[26] Mann, A. B., Shaheen, S., Maqbool, K., Poncet, S., "Fractional Burgers fluid flow due to metachronal ciliary motion in an inclined tube", Frontiers in physiology, 10, 588, (2019) DOI: https://doi.org/10.3389/fphys.2019.00588.

[27] Shaheen, S., Maqbool, K., Ellahi, R., Sadiq, M., Sait, "Metachronal propulsion of non-Newtonian viscoelastic mucus in an axisymmetric tube with ciliated walls", Communications in Theoretical Physics, 73(3), 035006, (2021) DOI 10.1088/1572-9494/abda1c.

[28] Oldroyd, J. G., "On the formulation of rheological Equations of state", Proceedings of the Royal Society of London. Series A. Mathematical and Physical Sciences, 200 (1063), 523-541, (1950) DOI: https://doi.org/10.1098/rspa.1950.0035.

[29] Podlubny, I., "Fractional differential Equations: an introduction to fractional derivatives, fractional differential Equations, to methods of their solution and some of their applications", Elsevier, (1998).

[30] Alsaadi, M. M., Habib, S. S., Al Muqhem, B. A., AlDrees, A., M., AlZamil, J., F., AlSadoon, H., A., "Significance of fractional exhaled nitric oxide measurements in detecting primary ciliary dyskinesia in Saudi children", Saudi Med J, 34 (1), 24-28, (2013). DOI: https://doi.org/info:doi/.

[31] Adomian, G., "Solving frontier problems of physics: the decomposition method", Springer Science & Business Media (Vol. 60)., (2013) DOI: https://doi.org/10.1007/978-94-015-8289-6.

[32] Az-Zo'bi, E., A., "On the reduced differential transform method and its application to the generalized Burgers-Huxley Equation", Applied Mathematical Sciences, 8 (177), 8823-8831, (2014) DOI: http://dx.doi.org/10.12988/ams.2014.410835.

[33] Az-Zo'bi, E., A., "An approximate analytic solution for isentropic flow by an inviscid gas model", Archives of Mechanics, 66 (3), 203-212, (2014).

[34] Az-Zo'bi, E. A., Shah, R., Alyousef, H. A., Tiofack, C., G., L., El-Tantawy, S., A., "On the feed-forward neural network for analyzing pantograph equations", AIP Advances, 14 (2), (2024) DOI: https://doi.org/10.1063/5.0195270.

[35] Az-Zo'bi, E. A., Shah, R., Alyousef, H. A., Tiofack, C., G., L., El-Tantawy, S., A., "On the feed-forward neural network for analyzing pantograph equations", AIP Advances, 14 (2), (2024) DOI: https://doi.org/10.1063/5.0195270.

[36] Az-Zo'bi, E., Akinyemi, L., & Alleddawi, Ahmed, O., "Construction of optical solitons for conformable generalized model in nonlinear media", Modern Physics Letters B, 35 (24), 2150409, 2021 DOI: https://doi.org/10.1142/S0217984921504091.

[37] Chatelin, R., Poncet, P., "A parametric study of mucociliary transport by numerical simulations of 3D non-homogeneous mucus", Journal of biomechanics, 49 (9), 1772-1780, (2016) DOI: https://doi.org/10.1016/j.jbiomech.2016.04.009.

[38] Chateau, S., d'Ortona, U., Poncet, S., Favier, J., "Transport and mixing induced by beating cilia in human airways", Frontiers in physiology, 9, 161, (2018) DOI: https://doi.org/10.3389/fphys.2018.00161.

[39] Shapiro, A. H., Jaffrin, M. Y., Weinberg, S. L., "Peristaltic pumping with long wavelengths at low Reynolds number", Journal of fluid mechanics, 37(4), 799-825, (1969) DOI: 10.1017/S0022112069000899.

[40] Choudhury, A., Filoche, M., Ribe, N. M., Grenier, M., Dietze, G., F., "On the role of viscoelasticity in mucociliary clearance: a hydrodynamic continuum approach", Journal of Fluid Mechanics, 971, A33, (2023). DOI: 10.1017/jfm.2023.682.

BIOGRAPHIES

Dr. Khadija Maqbool is a dedicated faculty member in the Department of Mathematics & Statistics, currently serving as an Assistant Professor of Mathematics. She earned her PhD in Fluid Dynamics from Quaid-i-Azam University, Islamabad, and her research interests encompass Heat and Mass Transfer Analysis, Mathematical Modelling of Bio fluid Flows, and the application of Integral Equations in fractional calculus, among others. With over 50 publications in prestigious peer-reviewed journals, Dr. Maqbool has established herself as a prominent researcher in her field.

Ms. Hajra Ansar is a research student in the Department of Mathematics & Statistics, and earned her MS degree in Mathematics. Ms. Hajra has interest in applied mathematics and expertise in modelling and solving the mathematical problems.

Amer Bilal Mann is an Assistant Professor Mathematics and completed his PhD from Quaid-I-Azam University, Islamabad in 2010. His research interests are in the areas of cilia motion, wave scattering and mathematical physics including analytical and numerical methods for nonlinear differential equations. He is reviewer of many reputed international journals and also published several research papers. He has supervised BS and MPhil students also.

Sébastien Poncet is a Professor in the mechanical engineering department at Université de Sherbrooke (Canada) and holder of the NSERC chair on industrial energy efficiency. He obtained his PhD thesis in 2005 and his habilitation thesis in 2014 from Aix-Marseille University (France) on the stability, turbulence and heat transfer in rotating flows. His research activities cover many fields related to thermofluids including biological flows in human airways. He is the coauthors of more than 450 publications whose 170 in international journals.

List of figures:

List of Tables:

Symbols	**Definitions**	**Units**
a	mean tube radius	m
c	wave speed	m/sec
e	eccentricity of the elliptical path	
Fr	frictional force	**N**
h	amplitude of the wave	m
J	differential operator	
k	summation index	
P	fluid pressure	N/m^2
q	Flux	m/sec
Q	volume flow rate	m^3/sec
$\overline{Q}$	mean volume flow rate	m^3/sec
r, z	cylindrical coordinates in fixed frame	m
R, Z	cylindrical coordinates in wave frame	M
Re	Reynolds number	
S	extra stress tensor	N/m^2
t	Time	Sec
u, w	velocity components in fixed frame	m/sec
U, W	velocity components in wave frame	m/sec

Greek Letters

Greek letter	Abbreviation	**Units**

α, β	fractional parameters	
β^*	ratio of mean tube radius to wavelength	
ε	cilia length	M
θ_1	retardation time of Oldroyd-B fluid	S
λ	Wavelength	M
λ_1	relaxation time of Oldroyd-B fluid	S
μ	fluid viscosity	kg/ (m.s)
ρ	fluid density	kg/m^3
Ψ	stream function	kg/ (m.s)
Γ	Incomplete gamma function	

Table 1:

Fluid Models	**Rheological Properties**	**dp/dz**
Frac Oldroyd-B	$\lambda_1=1$, $\theta_1=0.7$, $\alpha=\beta=0.5$	0.723073
Oldroyd-B	$\lambda_1=1, \theta_1=0.7, \alpha=\beta=1$	0.615308
Frac Maxwell	$\lambda_1=1, \theta_1=0, \alpha=\beta=0.5$	0.370013
Maxwell	$\lambda_1=1, \theta_1=0, \alpha=\beta=1$	0.295904

Figures

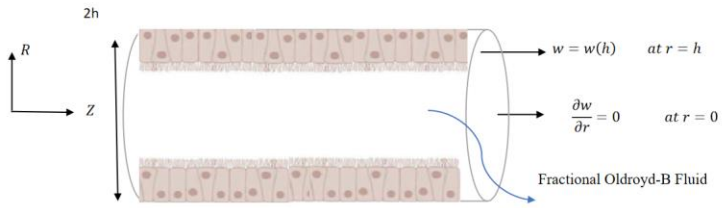

Figure 1

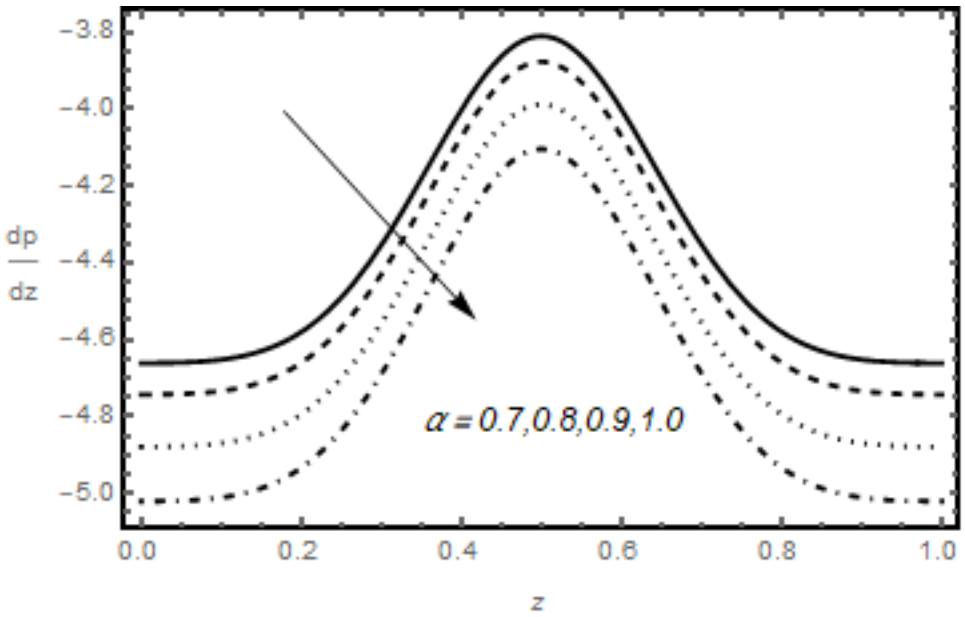

Figure 2a

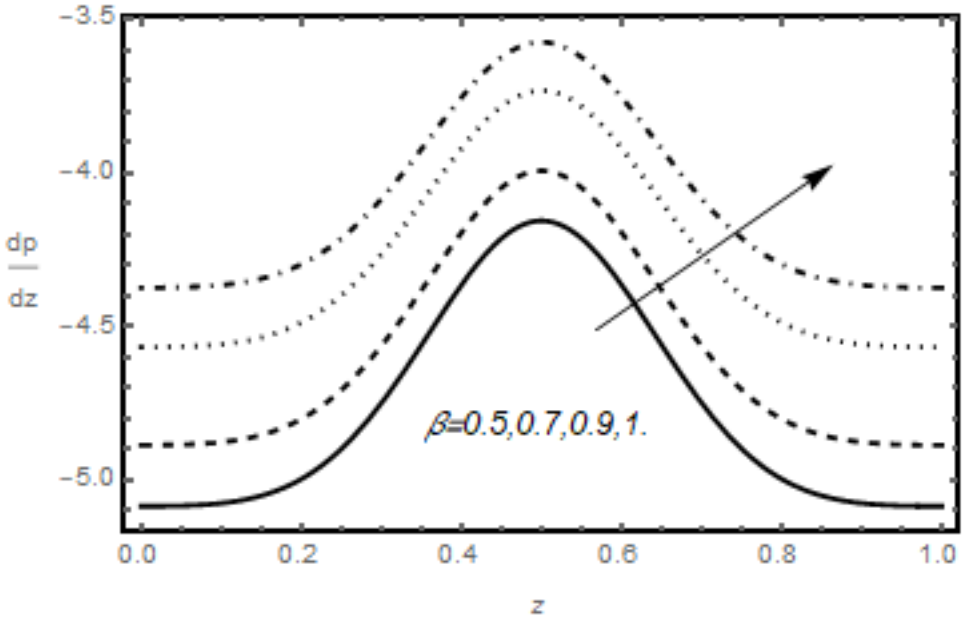

Figure 2b

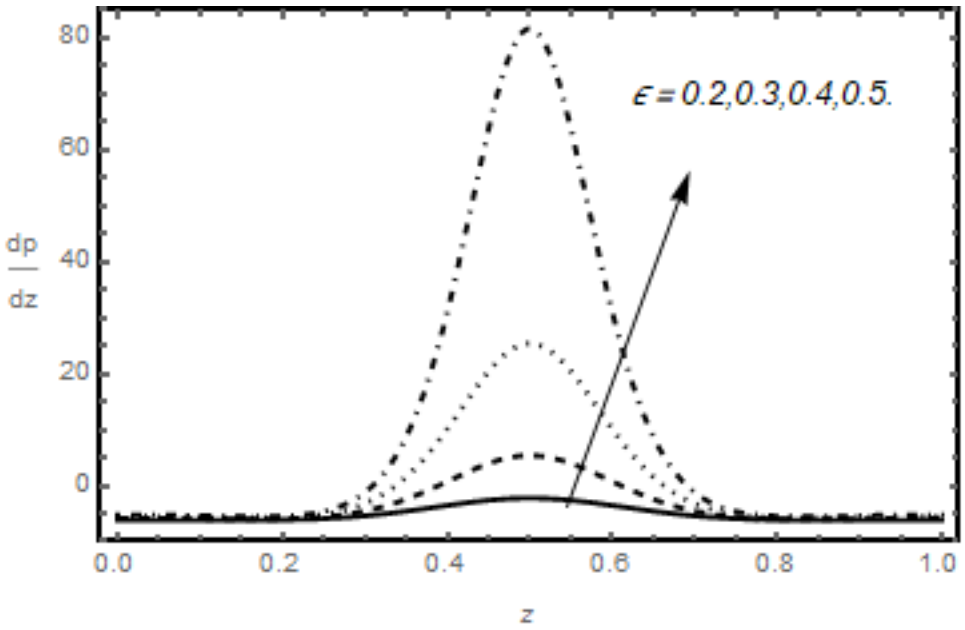

Figure 2c

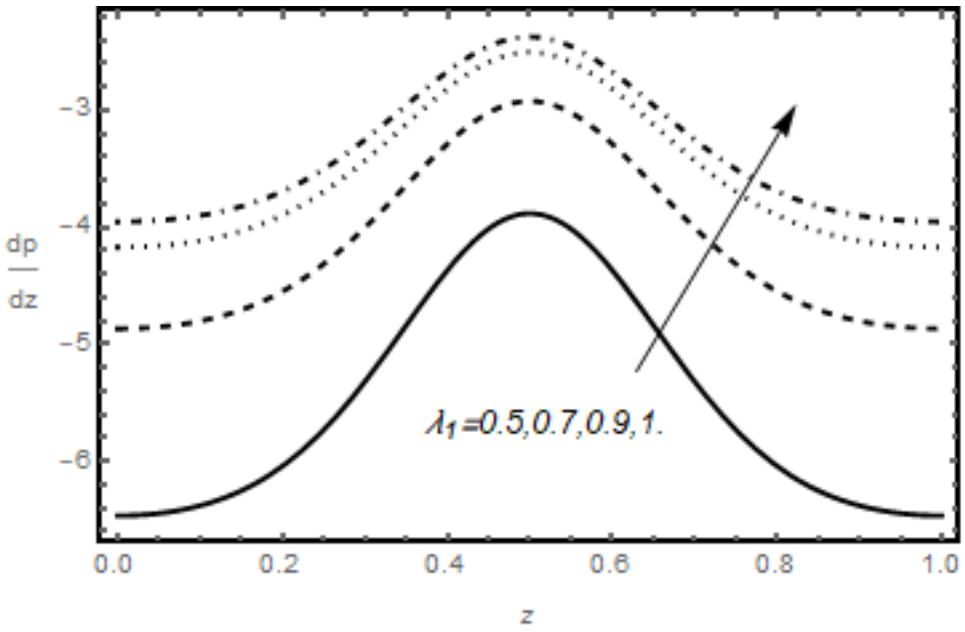

Figure 2d

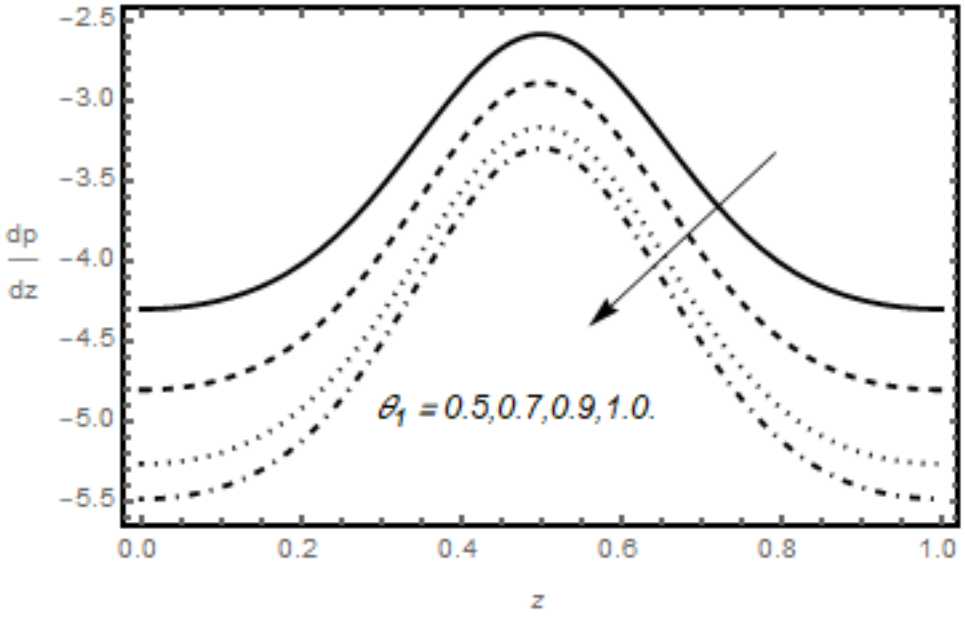

Figure 2e

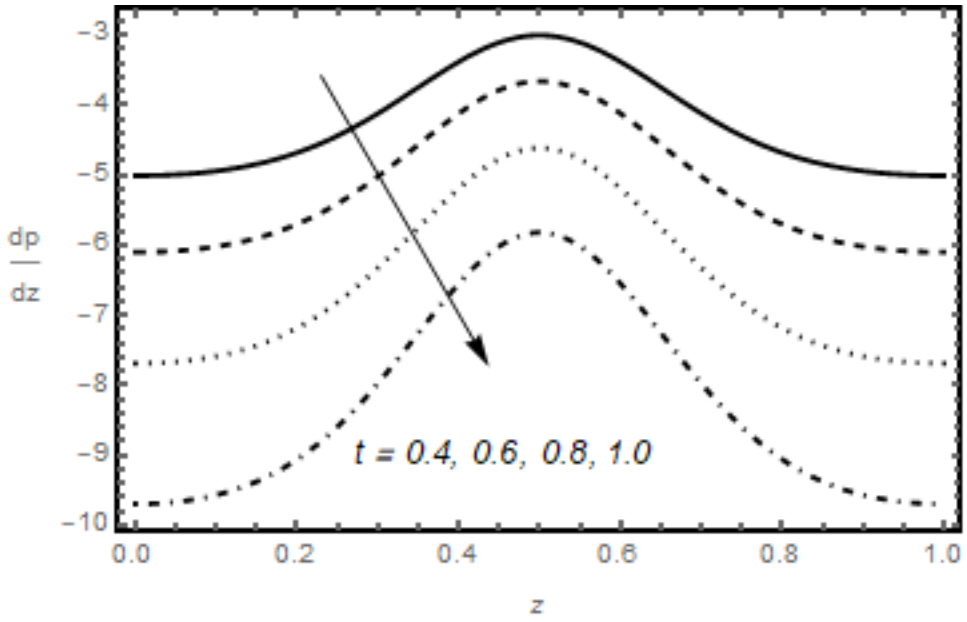

Figure 2f

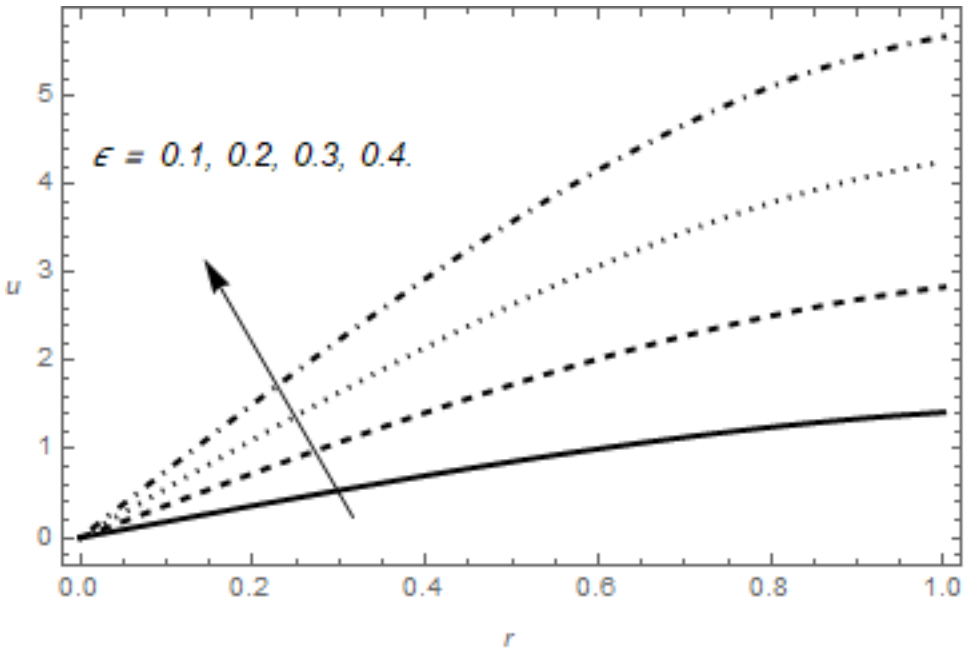

Figure 3a

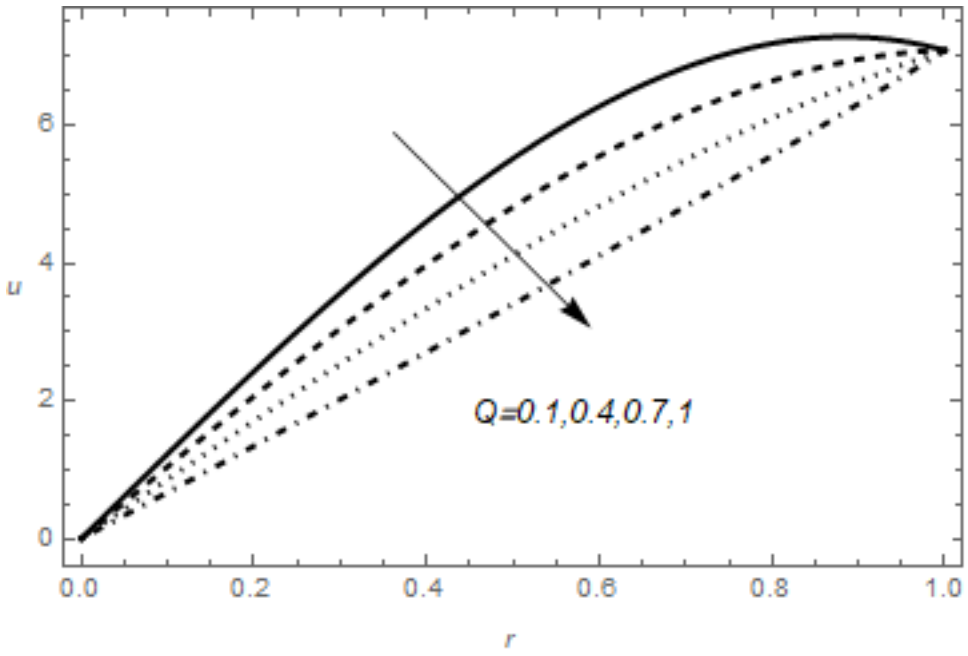

Figure 3b

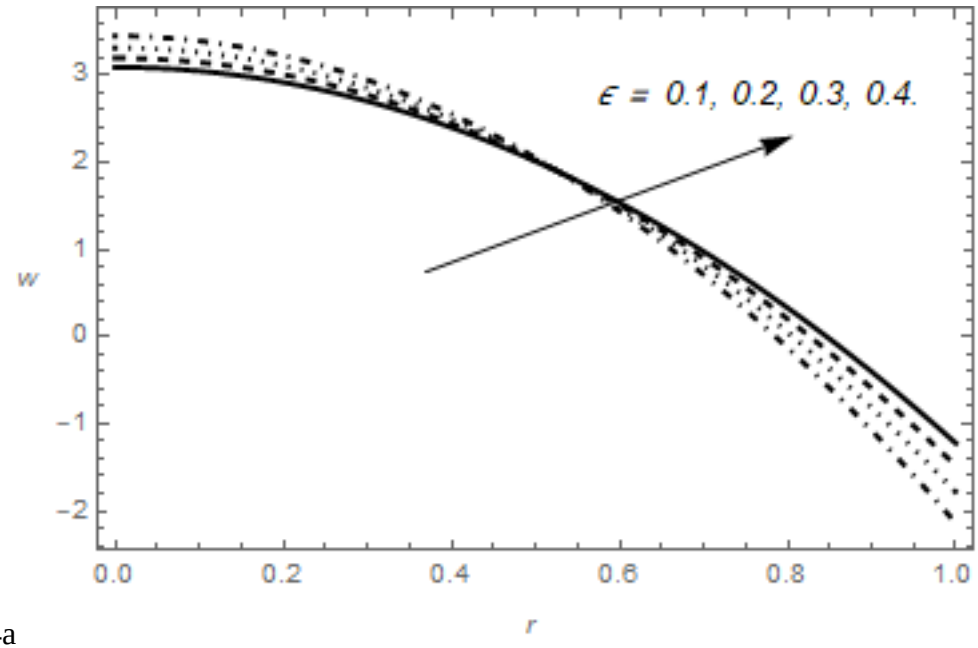

Figure 4a

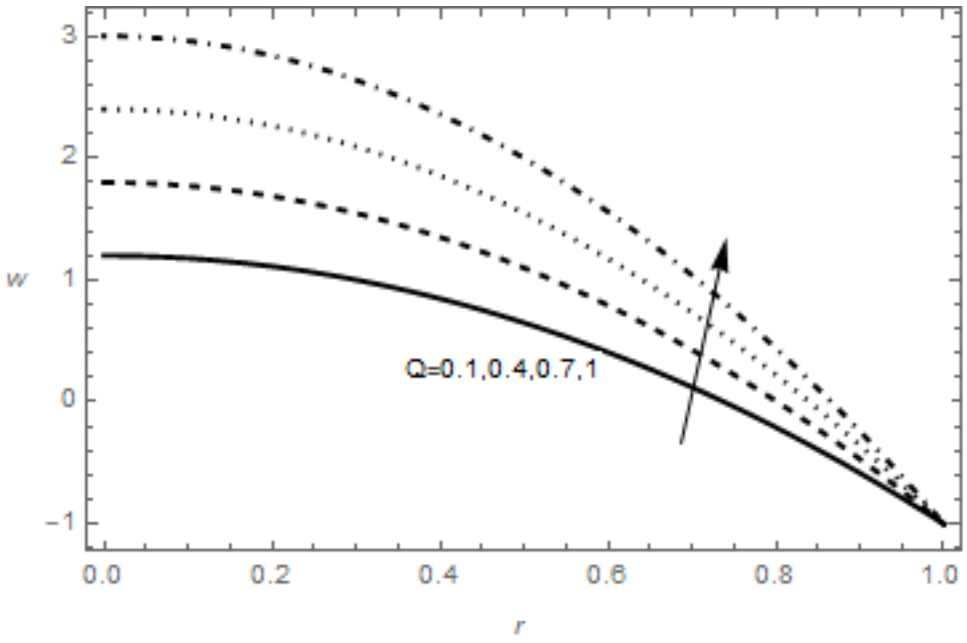

Figure 4b

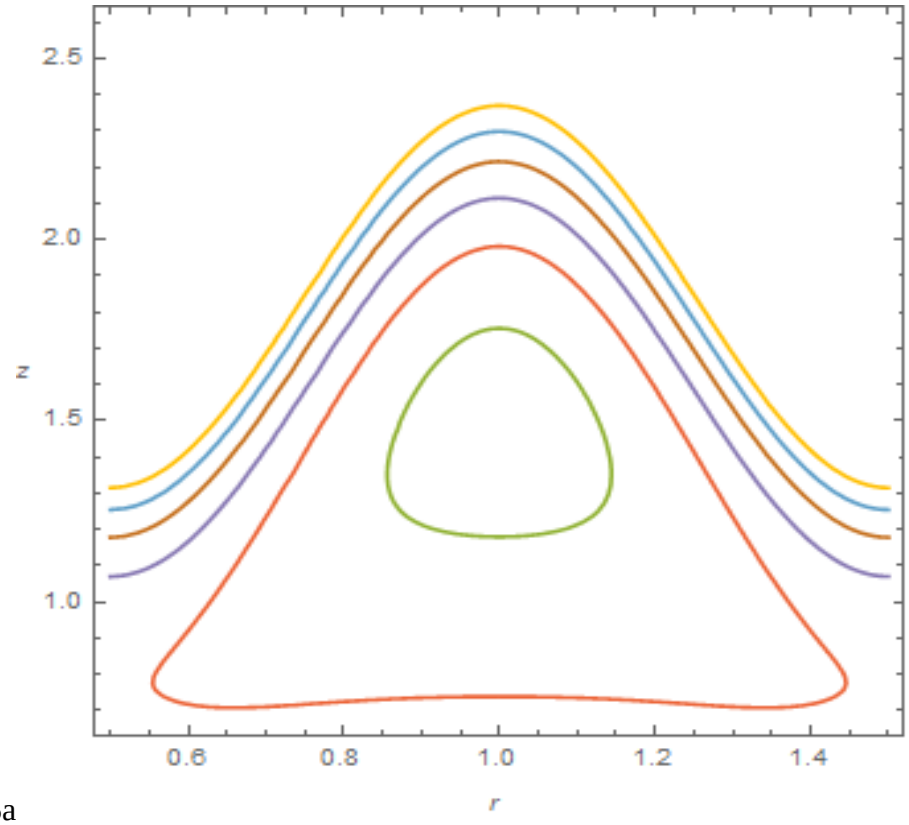

Figure 5a

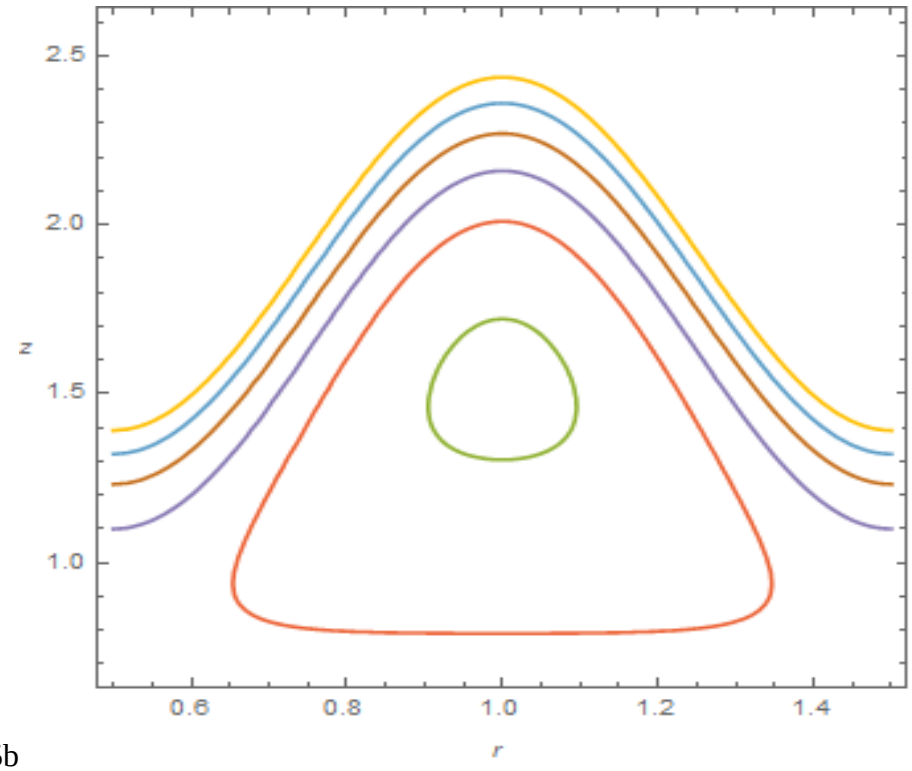

Figure 5b

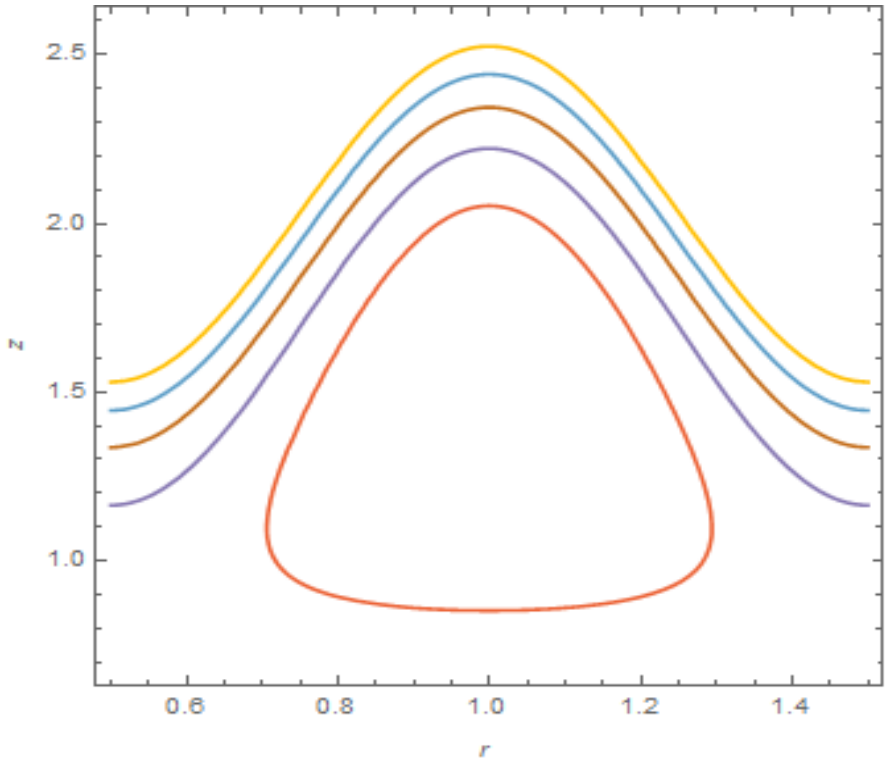

Figure 5c

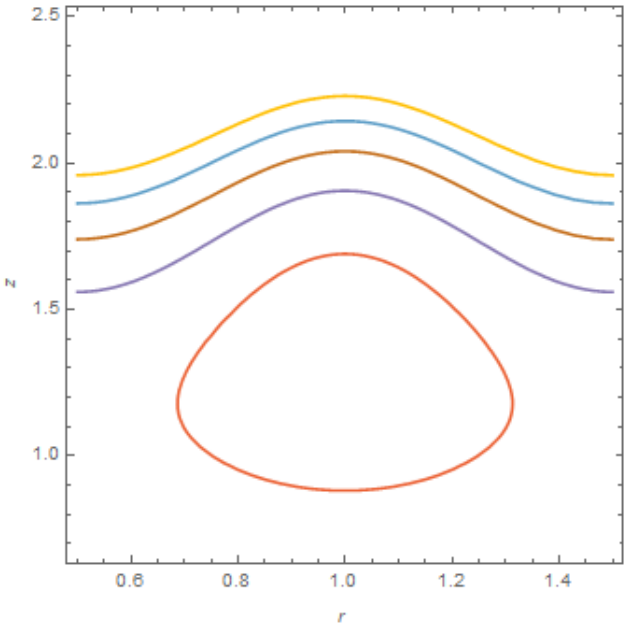

Figure 6a

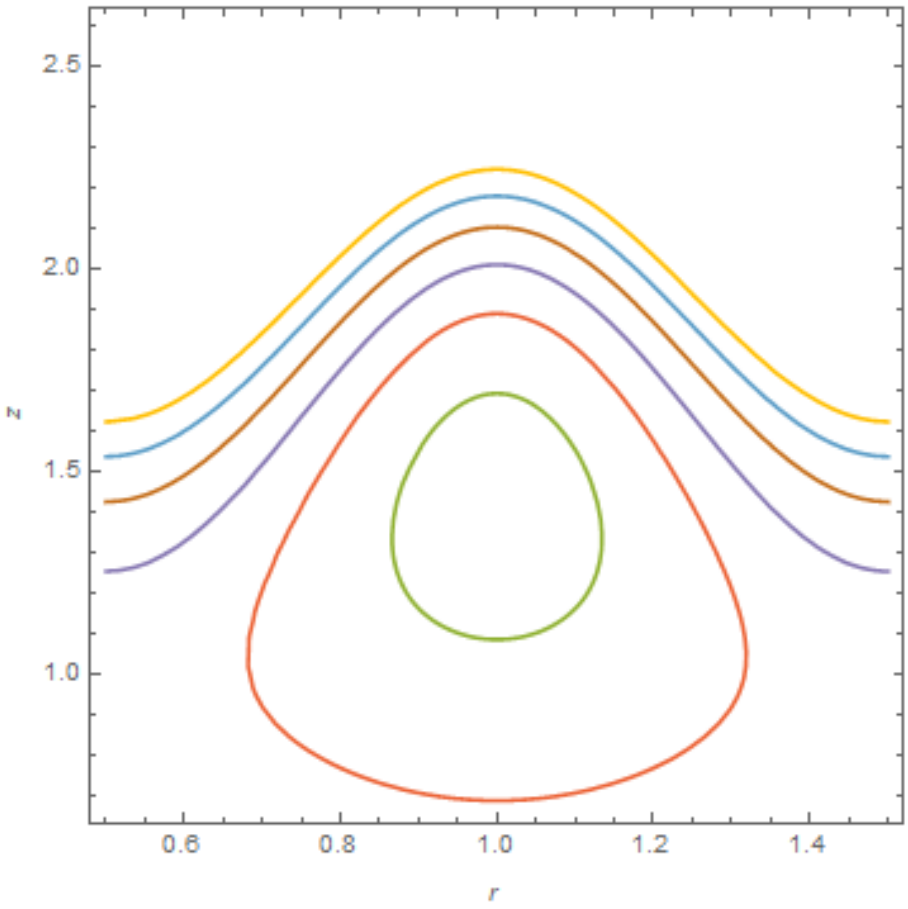

Figure 6b

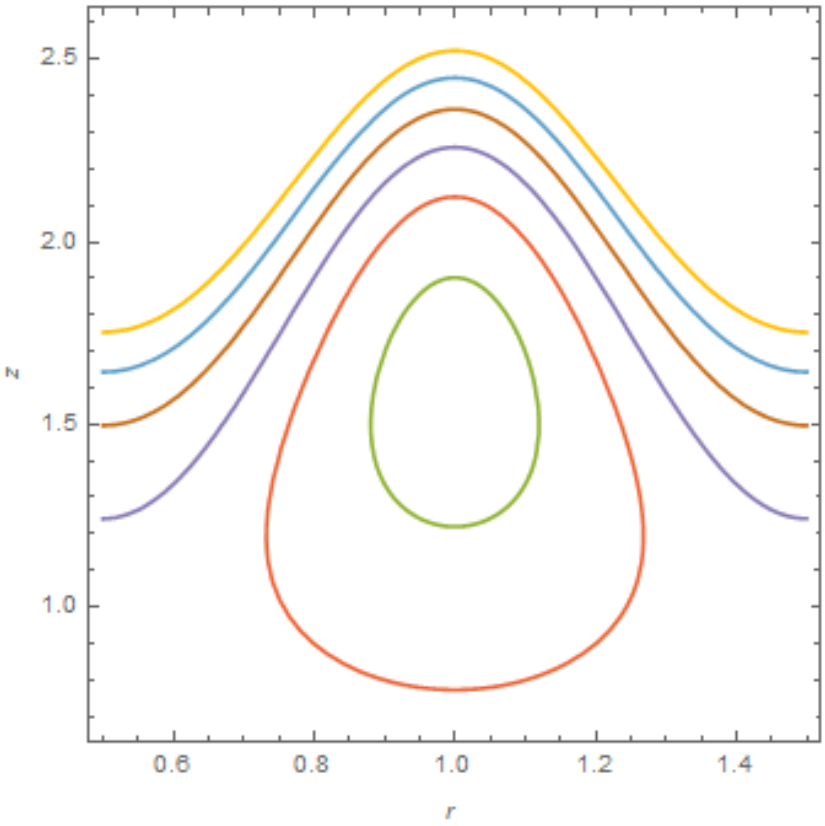

Figure 6c

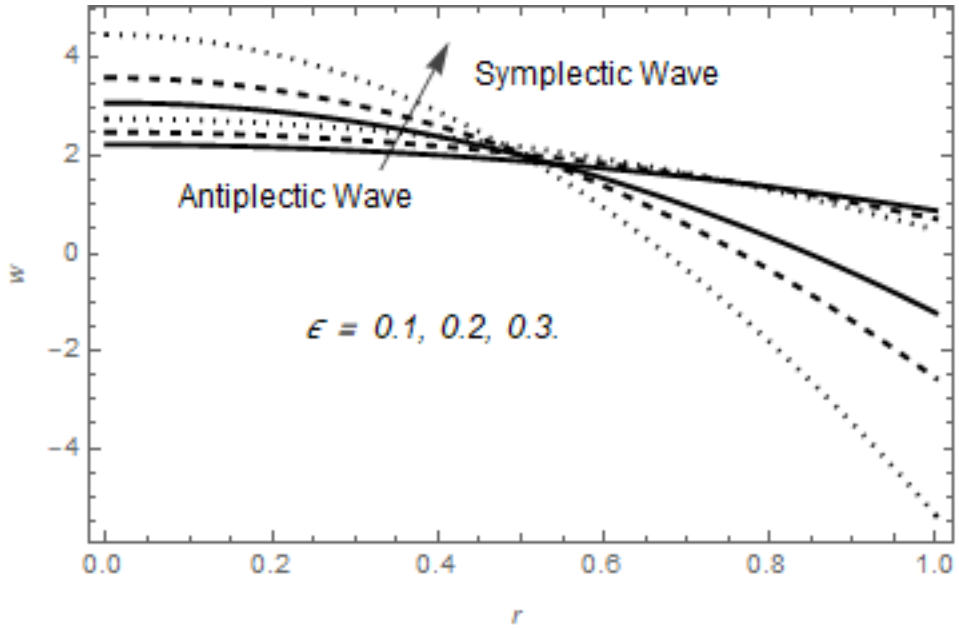

Figure 7a

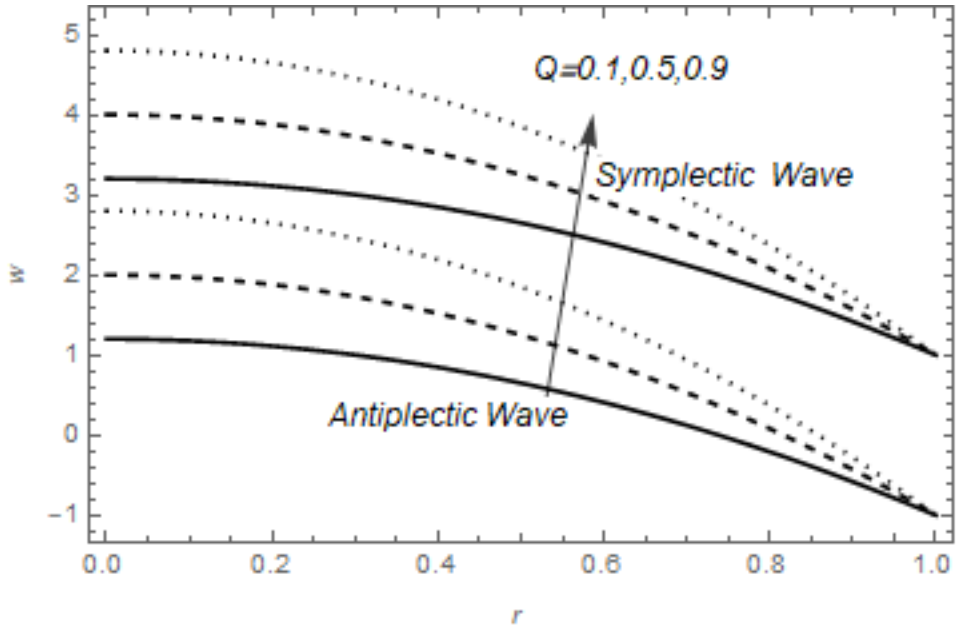

Figure 7b